

HOSTED BY



ELSEVIER

Contents lists available at ScienceDirect

# Engineering Science and Technology, an International Journal

journal homepage: [www.elsevier.com/locate/jestch](http://www.elsevier.com/locate/jestch)

Full Length Article

## Physical study of the impact of injector design on mixing, convection and turbulence in ladle metallurgy

Prince Gajjar<sup>a,b,\*</sup>, Tim Haas<sup>b</sup>, Kwaku Boateng Owusu<sup>a,b</sup>, Moritz Eickhoff<sup>b</sup>, Pruet Kowitzarangkul<sup>a</sup>, Herbert Pfeifer<sup>b</sup>

<sup>a</sup>The Sirindhorn International Thai-German Graduate School of Engineering (TGGS), King Mongkut's University of Technology North Bangkok (KMUTNB), Bangkok 10800, Thailand

<sup>b</sup>Department for Industrial Furnaces and Heat Engineering (IOB), RWTH Aachen University, Kopernikusstraße 10, 52074 Aachen, Germany

### ARTICLE INFO

#### Article history:

Received 7 August 2018

Revised 14 November 2018

Accepted 21 November 2018

Available online xxxxx

#### Keywords:

Bulk convection

Injector design

Ladle metallurgy

Mixing time

Turbulent kinetic energy

### ABSTRACT

Mixing time is a common measure to evaluate the efficiency of homogenization in ladle metallurgy. In this study, a 1:3 scale water model of a 185 t industrial gas-stirred ladle with an eccentric porous plug at the bottom is used to study the impact of different injector designs on mixing at a constant flow rate of 16.7 slm (standard liter per minute) at the pressure of 2 bar and filling height of 1.076 m. For that, the mixing time is measured with a continuous food color injection, accompanied by Particle Image Velocimetry (PIV) to correlate the results with the bulk convection and the turbulent kinetic energy. The results show that all tested injectors yield similar mixing times with a relative deviation of 6.4%. It is therefore concluded that the injector design plays a minor role in the optimization of ladle metallurgy.

© 2018 Karabuk University. Publishing services by Elsevier B.V. This is an open access article under the CC BY-NC-ND license (<http://creativecommons.org/licenses/by-nc-nd/4.0/>).

### 1. Introduction

To satisfy the current demand for steel products, world crude steel production reached 1691.2 million tones for 2017, up by 5.3% compared to 2016 [1]. According to the World Steel Association (worldsteel) [2], the crude steel capacity utilization ratio<sup>1</sup> in May 2018 was 77.7%. The ratio is 4.2% higher than that of May 2017. This indicates the increasing requirement of steel products. Driven by this increasing demand for quality steel, secondary metallurgical processes (i.e. refining treatment in a steel ladle) are becoming increasingly important in steelmaking. The functions of ladle metallurgy include alloying, homogenization, deoxidation, vacuum degassing, decarburization, desulfurization, inclusion removal and temperature control. To optimize the steelmaking process, ladle purging with argon gas has been utilized since it was universally adopted in the 1960s.

\* Corresponding author at: The Sirindhorn International Thai-German Graduate School of Engineering (TGGS), King Mongkut's University of Technology North Bangkok (KMUTNB), Bangkok 10800, Thailand and Department for Industrial Furnaces and Heat Engineering (IOB), RWTH Aachen University, Kopernikusstraße 10, 52074 Aachen, Germany.

E-mail address: [prince.g-pe2016@tggs.kmutnb.ac.th](mailto:prince.g-pe2016@tggs.kmutnb.ac.th) (P. Gajjar).

Peer review under responsibility of Karabuk University.

<sup>1</sup> The monthly crude steel capacity utilization ratio is calculated based on crude steel production information available at World Steel Association (worldsteel) and Organization for Economic Co-operation and Development (OECD) capacity estimates (see Appendix for more details).

Progressive modifications are taking place intermittently in the field of purging gas ladles. The argon injection at the bottom of the ladle promotes the homogenization of the chemical constituents and temperature. The interaction between the flow of molten steel and rising gas bubbles results into the effective mixing of the additives (either desulfurizing agents or alloying elements) and molten steel and enhances the chemical reactions by bringing reactants in close proximity of each other. However, the bubble-induced flow can also cause the reoxidation of molten steel, slag entrapment, and refractory erosion. Many industrial manufacturers and researchers consider the mixing time, i.e. the time required for the homogenization of the composition, as the indicator of the state of agitation of the fluid inside a reactor [3–5]. It is, therefore, a popular measure of the process performance of gas stirred ladles. The mixing time is influenced by two transport mechanisms [6]: (i) bulk or convective flow which is the macroscopic recirculation generated by the upward gas plume and (ii) eddy or turbulent diffusion which occurs due to the dissipation of the turbulent kinetic energy of the system.

Nakanishi et al. [7] were first to correlate the mixing time with the specific rate of energy input in a water model (length to diameter ratio = 1.1) of an argon stirred ladle. The results indicate no influence of vessel's shape, size, and mode of energy input on the mixing behavior. The mean value of data is represented by the empirical correlation:

<https://doi.org/10.1016/j.jestch.2018.11.010>

2215-0986/© 2018 Karabuk University. Publishing services by Elsevier B.V.

This is an open access article under the CC BY-NC-ND license (<http://creativecommons.org/licenses/by-nc-nd/4.0/>).

Please cite this article as: P. Gajjar, T. Haas, K. B. Owusu et al., Physical study of the impact of injector design on mixing, convection and turbulence in ladle metallurgy, Engineering Science and Technology, an International Journal, <https://doi.org/10.1016/j.jestch.2018.11.010>

$$\tau_m = 800\varepsilon_m^{-0.4} \quad (1)$$

$$\varepsilon_m = 0.028 \frac{5QT}{W_g} \log\left(1 + \frac{Z}{148}\right) \quad (2)$$

where  $\tau_m$  is the time in seconds required to attain complete mixing,  $\varepsilon_m$  is the rate of dissipation of energy (W/t), Q is the flow rate of argon gas (1/min/NTP), T is the absolute temperature (K),  $W_g$  is weight of bath (t) and Z is height of the melt (cm).

Multiple studies have confirmed the work of Nakanishi et al. [7], and they have also shown that the dimensions of the ladle and tracer injection position affect the measured mixing time. These studies are summarized in Table 1 [3,8]. In most studies, the mixing time was defined as the duration to gain a degree of homogeneity of 95% [3,9–14]. In contrast to that, Krishnamurthy et al. [15] and Asai et al. [16] set the degree of homogeneity above 99.7% in their research. To achieve highest mixing efficiency, a bath aspect ratio close to 1–1.5 was suggested [3,5,9,13,16–20]. Several studies indi-

cated that the mixing time decreases with increasing flow rate [9,10,12,15,16,19,21–23]. However, this effect is diminished at higher gas flow rates [12,16,19]. Initially, it was concluded that mixing time is independent of tracer injection position [15], but later it was shown that tracer addition and monitoring position affects the measured mixing time [9,18,24]. Furthermore, mixing time decreased when the tracer amount was increased [25]. Deeper immersion of the tracer injector enhances the recirculation velocity, which reduces the mixing time [19,26].

The mixing time is affected by the position of plugs and number of plugs used [9,23,24]. Mixing time decreases with decreasing plug diameter [15]. At high or medium gas flow rates, the mixing time slightly increases with an increase in the number of plugs, while the opposite behavior was observed at low gas flow rates [11]. Two types of circulation zones were found in ladles with dual plugs: in the middle between the two plumes and between plume and sidewall [27]. For a shorter mixing time, dual blowing plugs were preferred to center blowing or eccentric blowing with a single

**Table 1**  
Summary of mixing time measurement experiments reported in literature.

Year	Investigators	Mixing time correlation, $\tau_m$	Specific energy, $\varepsilon_m$ [W/kg]	Vessel dimensions [m]	Specific gas flow rates, Q [m <sup>3</sup> /min/T]	Mixing criteria [%]	Mass of fluid [kg]	Experimental Technique
1975	Nakanishi et al. [7]	$\tau_m = 800\varepsilon_m^{-0.402}$	0.001–0.004	D = 0.419; L = 0.465; L/D = 1.110	0.015–0.06		64	pH
1983	Sano & Mori [33]	$\tau_m = 274\varepsilon_m^{-0.33}R^{1.33}L^{-0.673}$						Theoretical
1983	Asai et al. [16]	$\tau_m = 274\varepsilon_m^{-0.33}R^{1.36}L^{-1.0}$	0.001–0.060	D = 0.405, 0.20, 0.10; L/D = 0.5 to 1		99.9%	52 (max) & 0.4 (min)	Electrical conductivity
1985	Sinha & McNallan [18]	$\tau_m = 692\varepsilon_m^{-0.89}$	0.002–0.037	D = 0.45; L = 0.48; L/D = 1.067	0.02–0.4	97.7%	76	pH
1986	Mazumdar & Guthrie [12]	$\tau_m = 37\varepsilon_m^{-0.33}R^{1.66}L^{-1.0}$	0.006–0.022	D = 1.12; L = 0.5 to 1.10	0.012–0.06	95% bulk	1000	Electrical conductivity
1987	Stapurewicz & Themelis [14]	$\tau_m = 164\varepsilon_m^{-0.39}L^{0.39}$	0.015–0.085	D = 0.66; L = 0.675 to 1.008	0.13–0.96	95%	310 (max)	Photocell
1988	Mietz & Oeters [34,35]	$\tau_m = CQ^{-n4}$	0.012–0.046	D = 0.63; L = 0.58	0.038–0.29	95%	311	Electrical conductivity & colorometry
1988	Krishnamurthy et al. [15]	$\tau_m = CQ^{-n5}$	0.012–0.194	D = 0.48; L = 0.10 to 0.45; L/D = 0.921	0.11–2.67	99.9%	81 (max)	Electrical conductivity
1995	Zhu et al. [9]	$\tau_m = 8.52\varepsilon_m^{-0.33}N^{0.336}$	0.005–0.010	D = 0.4; L = 0.4; L/D = 1.000		95%		Electrical conductivity
1995	Mandal et al. [23]	$\tau_m = 15Q^{-0.38}R^{2.0}L^{-0.567}$	0.007–0.010	D = 0.6, 0.45, 0.3; L/D = 0.8 to 1.2		95%		Electrical conductivity
1998	Iguchi et al. [10]	$\tau_m = 1200Q^{-0.47}D^{1.97}L^{-1}\nu_L^{0.478}$	0.012–0.094	D = 0.2; L = 0.25; L/D = 1.250		95%		Photocell CaCO <sub>3</sub> powder
			0.025–0.191	D = 0.14; L = 0.175; L/D = 1.250				
2014	Amaro-Villeda et al. [11]	$\tau_m = 9.83N^{0.1025}\varepsilon_m^{-0.364}\left(\frac{h_s}{R}\right)^{-0.0051}\left(\frac{h_s}{H}\right)^{0.0049}$	0.8	D = 0.537; L = 0.41; L/D = 0.76		95%		pH

<sup>2</sup>  $\tau_m$  = mixing time correlation and  $\varepsilon_m$  = Specific energy.

<sup>3</sup> R = Radius of the ladle, L = Height of the ladle.

<sup>4</sup> C and n are functions of tracer addition and monitoring locations and Q = Gas flow rate.

<sup>5</sup> C and n are functions of flow regime and liquid depth.

<sup>6</sup> N = number of nozzles (max 3).

<sup>7</sup> For two plugs at  $\pm 0.5 R$ .

<sup>8</sup> D = Diameter of the ladle, VL = For water and silicone oil of varying kinematic viscosity.

<sup>9</sup> N = Number of nozzles,  $\varepsilon_m$  = Specific energy input rate, r/R = Nozzle radial position,  $h_s$  = Thickness of oil in mm and H = Liquid depth in mm.

plug [22]. Shorter mixing times can be achieved by injecting gas through two porous plugs [28]. When a plug is close to the ladle sidewall, the flow will distort the plume toward that sidewall, increasing the shear force on the wall [24]. Owing to that, the mixing time, and the potential for hydrodynamic erosion of the ladle's refractories are increased. An eccentric plug location can be adapted to avoid dead zones [13]. To emulate the slag, oil was used as a top layer, but it was concluded that mixing time is not a good parameter for predicting the two-phase mass transfer except when the same plug pattern is considered [29]. The upper slag phase dissipates a part of the input energy rate and therefore it increases the mixing time [3,30]. Due to increased buoyancy and phase dispersion in the ladle, the mixing time decreased with increasing bath height [15,20,21]. The kinetic energy input does not contribute to mixing in the same way as buoyancy [18,31,32]. The kinetic energy, which is brought into the system by the flushing of the inert gas, is typically less than 5% in the overall energy balance [3]. In terms of stirring energy, mixing time decreases as stirring energy increases [11].

In this study, the impact of injector geometry on mixing time is investigated. For this purpose, different injector plate designs are

built and used with a water model to measure the mixing time under a constant flow rate. The measurements are accompanied by additional PIV measurements to show the effect of the flow field and the turbulent kinetic energy on mixing.

## 2. Material and methods

### 2.1. Construction of the physical model

A 185 t industrial gas-stirred ladle with single eccentric plug and slightly tapered walls was studied. The hydrodynamic model was scaled to a 1/3rd of its size and made of acrylic glass. To prevent visual distortion and maintain hydrostatic pressure balance, the cylindrical model was enclosed by an additional cuboid acrylic glass model. The gas supply system and measurement setup for the experiment and the top view of the water model are sketched in Fig. 1. The dimensions are provided in Table 2. Physical simulation can be used to predict the flow behavior in the real ladle. An air-water physical model that replicates the industrial ladle processes has proven to provide a comprehensive understanding of the real

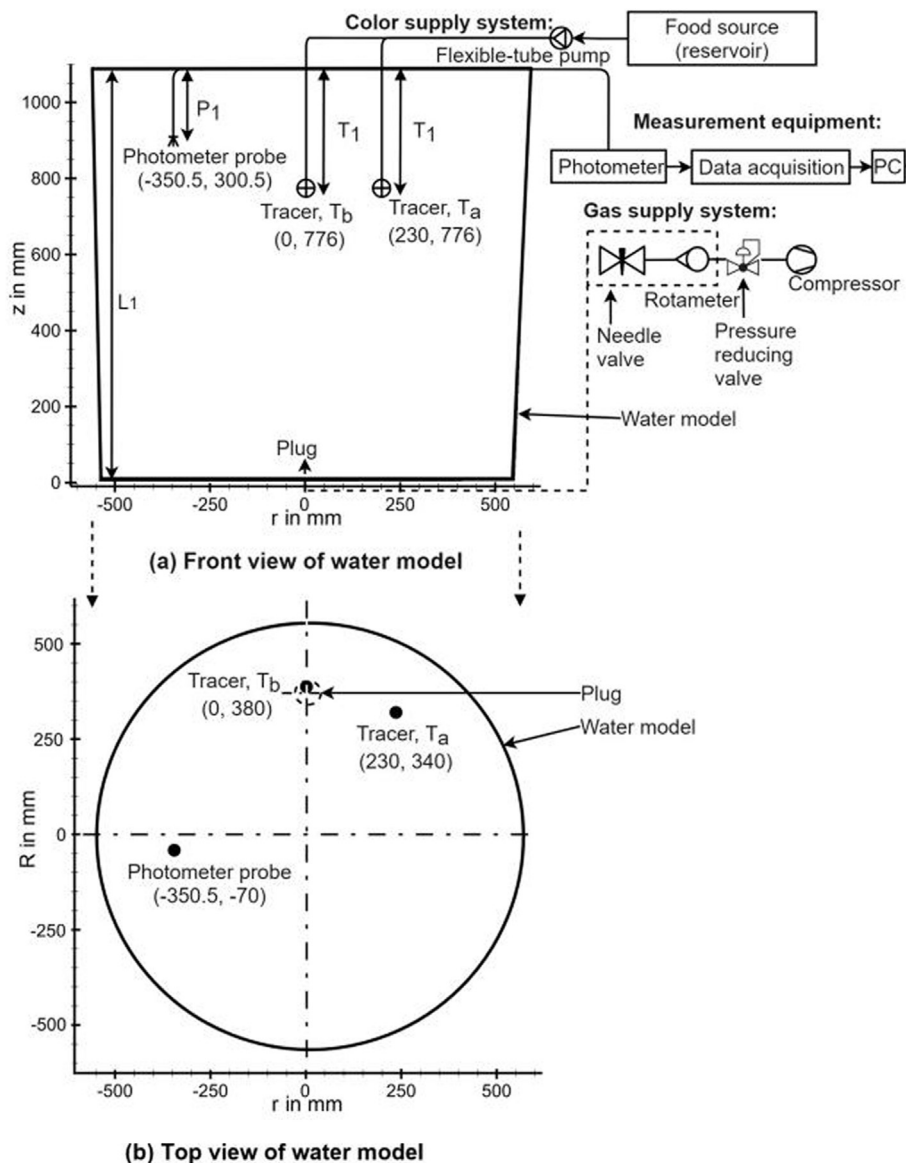


Fig. 1. Experimental setup. (a) Front view and (b) top view of the water model.

**Table 2**  
Employed properties and parameters (ladle and water model).

Parameter	Symbol	Prototype (185 t ladle)	1/3 scaled water model	Unit
Total height	$H_1$	3.8	1.28	m
Filling liquid height	$L_1$	3.23	1.076	m
Average diameter	$D_1$	3.245	1.081	m
Filling liquid volume	$V_1$	2.967	0.989	$m^3$
Porous plug diameter	$d_s$	0.29	0.09	m
Length to diameter ratio	$L_1/D_1$	0.9954	0.9954	
Liquid density (steel/water)	$\rho_l$	6932	998	$kg/m^3$
Gas density	$\rho_g$	0.8343	1.293	$kg/m^3$
The Depth of photometer probe	$P_1$	-	0.18	m
The Depth of tracer injector (hose)	$T_1$	-	0.3	m
The Eccentricity of the porous plug	$e$	1.05	0.35	m

system [36] since molten steel and water at room temperature have nearly equivalent kinematic viscosity [3,5].

2.2. Gas injector and volume flow

A standard porous plug of mullite ceramic ( $3Al_2O_3 \cdot 2SiO_2$ ), varied with five perforated plates made of polyvinyl chloride (PVC) of 5 mm thickness having different geometries (Fig. 2) is employed to investigate the influence on mixing time, bulk diffusion and flow field. Fig. 2 represents generalized diagram of all the perforated plates, and the details of the orifices are summarized in Table 3.

A compressor connected to a pressure regulator provides air at a constant gas flow rate. The compressed air is guided through a hose in the outer basin and is anchored to the bottom of the water model. A flowmeter controller (KROHNE Variable Area Flowmeter DK800) regulates the volume flow rate and a pressure regulator (Riegler 737.313 constant pressure regulator) allows for the adjustment of the volume flow rate of the stirring gas at 2 bar. Based on the float measuring principle, flowrate is regulated manually to

achieve the desired flow mark. The measuring unit consists of a calibrated glass cone in which a float moves up and down. The gas expands in the liquid because surrounding pressure is lower. Thus, the actual volume flow rate through the plug is higher. For each plug, the gas flow was regulated at 16.7 slm.

2.3. Particle image velocimetry (PIV)

Particle image velocimetry (PIV) is used to visualize the two-dimensional velocity field on the symmetry plane of the water model. A Neodymium-doped Yttrium Aluminum Garnet (Nd-YAG) laser is used for PIV. Light sheet optics is used to illuminate a plane in the water model, where the flow patterns are to be analyzed by adding polyamide particles doped with Rhodamine B as a tracer. A charge-coupled device (CCD) camera with a cut off-filter ( $\lambda_{cut-off}$ ) of wavelength 540 nm is used to track and evaluate the displacement of tracers. The maximum of the fluorescent spectrum of Rhodamine B ( $\lambda_{Rhodamine}$ ) is 584 nm, which is larger than  $\lambda_{cut-off}$ . Thus, only the fluorescent wavelength of the particles passes the filters and subsequently, the pictures show the particle patterns without the disturbance of scattered light. The experimental setup for the PIV measurements is shown in Fig. 3 [37]. The technical data of the PIV system are given in Table 4. The results were further processed using Davis 8 evaluation software.

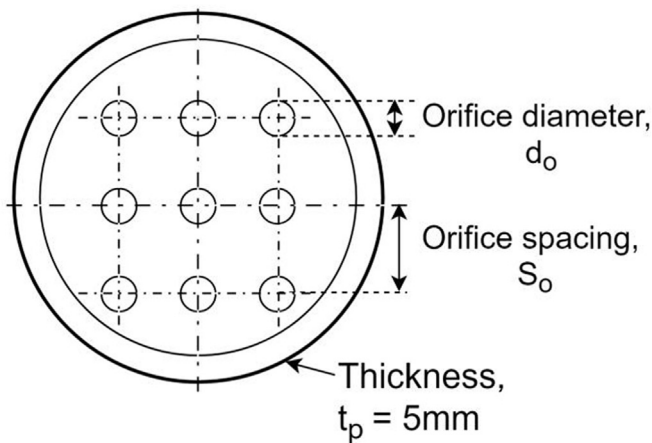


Fig. 2. Generalized representation of Geometry of various types of gas injectors.

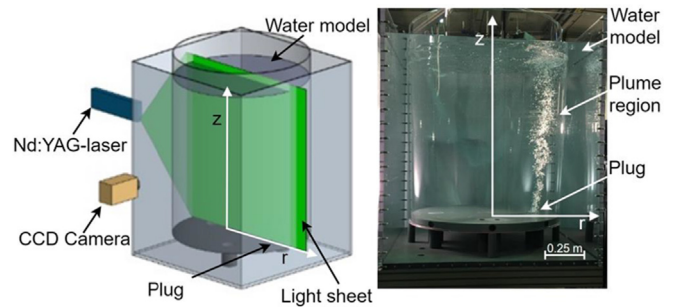


Fig. 3. PIV measurement setup and image of water model during the experiment.

**Table 3**  
Geometry of various types of gas injectors.

Case	Description	Number of orifices	Orifice diameter, $d_o$ [mm]	Orifice spacing, $S_o$ [mm]
I	Standard porous plug without any plates mounted	-	-	-
II	Porous plug mounted with a plate of reduced diameter	-	70	-
III	Porous plug mounted with a plate of 1 mm diameter orifices	$5 \times 5$	1	15
IV	Porous plug mounted with a plate of 2 mm diameter orifices	$5 \times 5$	2	15
V	Porous plug mounted with a plate of 3 mm diameter orifices	$5 \times 5$	3	15
VI	Porous plug mounted with a plate of 5 orifices in a single line	$1 \times 5$	2	15

**Table 4**  
Technical data of the PIV system.

Particular	Property	Symbol	Value	Unit
Nd-YAG-Laser	Wavelength	$\lambda_L$	532	nm
	Pulse energy	$E_L$	140	mJ
	Thickness of light sheet	$d_{LS}$	2–3	mm
	Pulse duration		4.3	ns
	Delay time between pulses	$t_{min}$	22,000	$\mu$ s
CCD camera	Resolution		2048 × 2048	px
	Frequency (double exposure)		5	Hz
Filter	Cut-off wavelength	$\lambda_{cut-off}$	540	nm
Tracer particles	Diameter	$d_p$	10–20	mm
	Density	$\rho_p$	1.19	kg/m <sup>3</sup>
		$\lambda_{Rhodamine}$	584	nm

#### 2.4. Tracer injection

Many researchers [7,38–40], have used salts such as sodium chloride (NaCl), hydrochloric acid (HCl), or potassium chloride (KCl) as a tracer. In each case, one mixing time was obtained for the defined scenario. In order to validate this mixing time and to correct for the deviations (e.g. by computing mean values), it was necessary to perform several experiments under the same conditions. Furthermore, the density difference between the injected salt solutions and the water in the model can lead to convection effects, which superimpose the mixing effects of the diffusion and the fluid flow [18]. In this study, these drawbacks are overcome by employing liquid food coloring as a tracer with continuous input and monitoring of the tracer. Firstly, there is almost no density difference between tracer and liquid, preventing convection effects, and secondly, a great number of independent mixing times are obtained in one experiment, lowering the standard deviation of the results [41].

After the quasi-stationary state of fluid flow is obtained, a tracer is injected via a peristaltic pump. The tracer consists of diluted blue water-soluble food coloring (Ruth, 7308-5000). A spectral photometer (Metrohm, Photometer 662) is used to determine the tracer concentration. The photometer measures the absorbance of the fluid flowing through the probe area using a photosensitive cell. The maximum of the absorbance spectrum is located at the wavelength ( $\lambda_{coloring}$ ) of 630 nm. The locations of the probe and tracer injection are given in Fig. 1. The photometer absorbance data were collected at the frequency of 5 Hz in a 'LabView' program. One additional measurement has been conducted in which the position of the tracer injection has been changed to observe its impact on the mixing time. A calibration procedure has been carried out to obtain the relation between measured absorbance and the concentration of the coloring. The calibration is done on a smaller scale to obtain precise results. A calibration curve determines the ideal concentration of a defined amount of food coloring in the water. The mixing time is ideally defined as the period required for the instantaneous tracer concentration to settle completely around the final tracer concentration in the bath. However, for this particular research this is not the usual definition. It takes several seconds before the first bulk of tracer reaches the probe and subsequently attains a linear range. After the food color injection is stopped, the bath concentration gradually becomes uniform and a constant concentration limit is observed. Fig. 4 shows a typical plot of the photometer signal with respect to the time measured during the experiment.

The method of continuous addition food color as a tracer differs from batch addition of the tracer to the water model. The measured absorption is compared with the concentration of the food color in the mixture. A linear regression is made to provide the function of the measured absorption and the required color con-

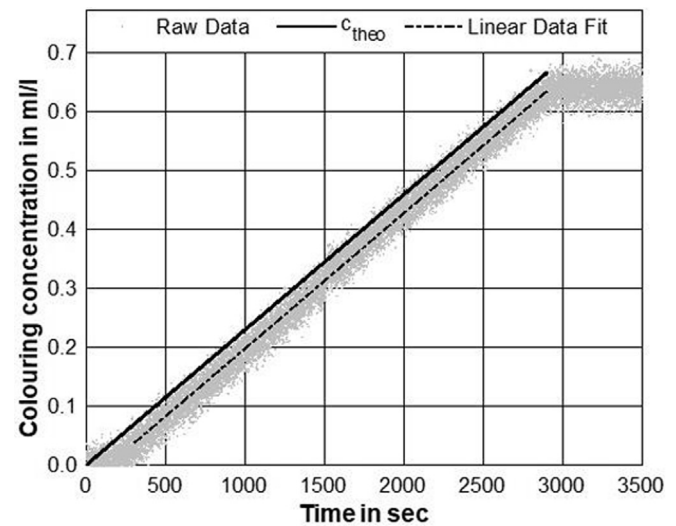


**Fig. 4.** Measured coloring concentration vs. time (for continuous injection of the tracer).

centration. The formula used to calculate the coloring concentration for the calibration and the theoretical concentration in the water model experiments is

$$c_{conc} = \frac{(i \cdot t \cdot \frac{m_{color}}{m_{water} + m_{color}})}{V_1 + t \cdot i} \quad (3)$$

where  $c_{conc}$  is the coloring concentration ( $ml_{color}/l_{water}$ ),  $i$  is the flow rate of pump ( $ml/s$ ),  $t$  is the time ( $s$ ),  $m_{color}$  is the food coloring in tracer ( $ml$ ),  $m_{water}$  is the water in tracer ( $ml$ ) and  $V_1$  is the filling liquid volume in ladle.

The measured values obtained with different injector configurations are processed similarly. The data in the linear part of the measurement signal shown in Fig. 4 can be expressed by

$$c_{fit} = m \cdot t + b \quad (4)$$

where  $c_{fit}$  is the fitted concentration of tracer ( $ml_{color}/l_{water}$ ),  $m$  is the slope of the plot ( $ml_{color}/l_{water} \cdot s$ ),  $t$  is time ( $s$ ) and  $b$  is y-axis intercept ( $ml_{color}/l_{water}$ ).

The gradient and y-axis intercept values of the above equation can be derived from linear regression. The slope of theoretical concentration is assumed to be equal to the slope of experimental concentration. Comparing the time of a given concentration in the experiment with the theoretically required time to reach this concentration, one can obtain a temporal difference which is defined as the mixing time. The mixing time can be calculated as

$$\tau_m = -\frac{c}{m} \quad (5)$$

where  $\tau_m$  is mixing time (s),  $c$  is y-axis intercept ( $ml_{\text{color}}/l_{\text{water}}$ ) and  $m$  is the slope of the plot ( $ml_{\text{color}}/l_{\text{water}} s$ ).

### 3. Results

#### 3.1. Mixing time

In the presented experiments, mixing times for different injector configurations were measured. For that, different perforated PVC plates were built into the injector used with the water model while retaining the gas flow rate ( $Q$ ) of 16.7 slm. The results are plotted in Fig. 5. It can be seen that all the injector configurations yielded similar mixing times with a relative deviation of 6.4%. The differences between the mixing times obtained with the standard porous plug with, or without a diameter reduction are negligibly small. The mixing times measured in the cases where PVC plates were used (Case II, III, IV, and V) are longer than in Case I and II. Case III and IV yield similar mixing times, about 7% longer than the porous plug cases. In Case V, that is to say, with 25 orifices of 3 mm arranged in a 5 by 5 pattern, the required mixing time is the longest. Among all the investigated gas injectors at the same conditions, the shortest mixing time is observed in Case II. In an additional experiment, the tracer position was changed and the mixing time for the Case IV configuration was measured again. As shown in Fig. 1, the tracer injection position was altered to the position vertically above the plume region in the ladle. The results are shown in Table 5. For the altered injection position, the experiment yielded a mixing time of more than double of that measured with the injection at the standard position. This is in agreement with various researchers [9,22,25], who found that the tracer position affects the mixing time.

#### 3.2. PIV: Bulk convection

In order to physically explain the observed mixing behavior, additional PIV measurements were conducted. Retaining a con-

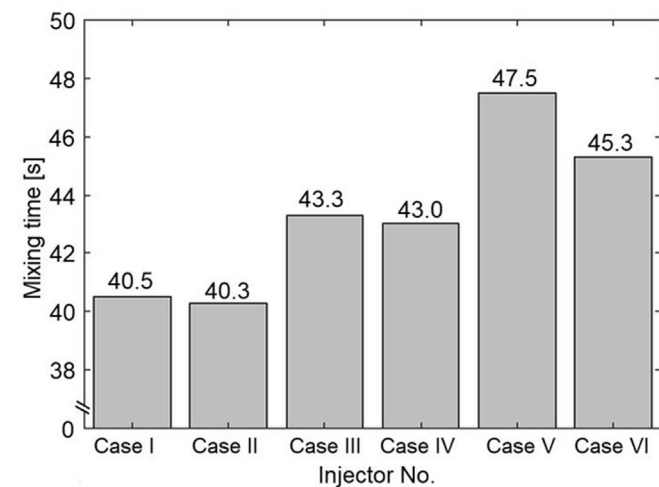


Fig. 5. Mixing time results.

Table 5  
Mixing time at various tracer positions in Case IV.

Tracer injection position	Description	Mixing time [s]
ta ( $r = 230$ mm; $z = 776$ mm)	Tracer injection position away from the plume trajectory	43.0
tb ( $r = 0$ mm; $z = 776$ mm)	Tracer injection position vertically above the plume	97.6

stant gas flow rate ( $Q$ ) of 16.7 slm, the flow fields were examined for all the investigated injector configurations. Fig. 6 presents the cross-section A-A which was investigated during the PIV measurements in the water model and the results of PIV are illustrated in Fig. 7.

Fig. 7 shows the velocity magnitude and direction on the main flow plane (symmetry plane), thereby providing information about the magnitude of the bulk convection. Since the bubble plume is very dense, the void fraction in this region is very high. Consequently, fewer tracers could be detected for the evaluation of the flow field. Thus, the evaluation becomes vague in the plume region ( $r = 350$  mm) and this region is not included in the subsequent discussion. Furthermore, the acrylic glass model is produced of two parts. Thus, an adhesive seam is present ( $r = -450$  mm), where the image is highly distorted. Therefore, many tracers are assigned incorrectly, yet again making the evaluation vague. Independent of the type of injector employed, the eccentric plug position results in one circulating flow extending over the whole ladle. Although the velocity in the plume region cannot be evaluated, it can be seen that the bulk liquid is moved upwards in this region. Reaching the free surface, the flow is redirected radially away from the

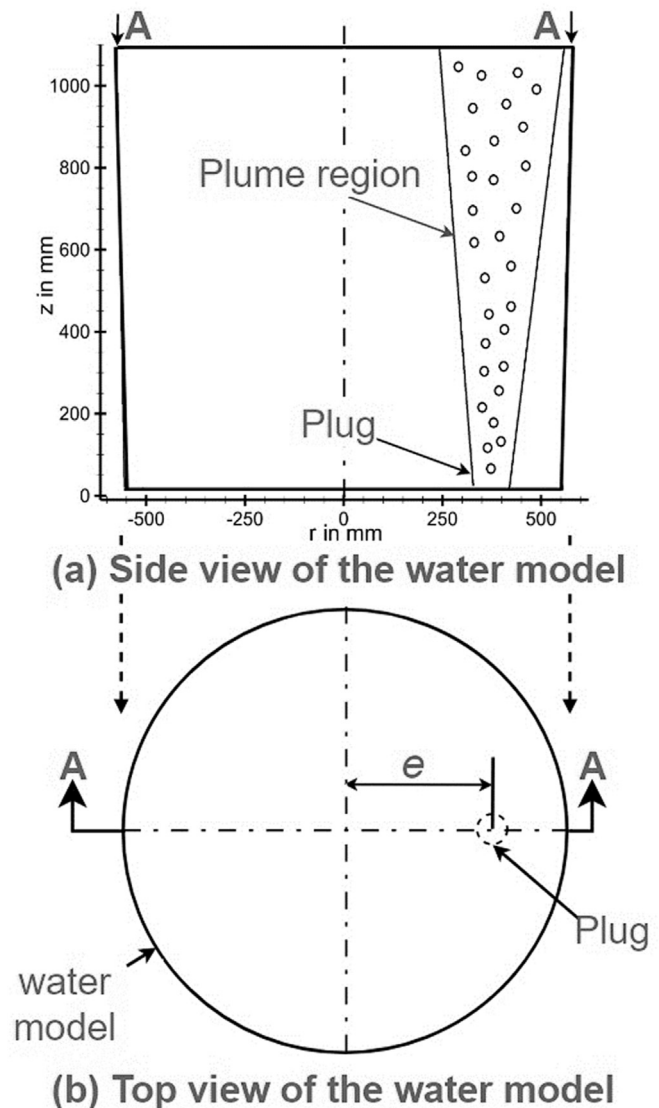
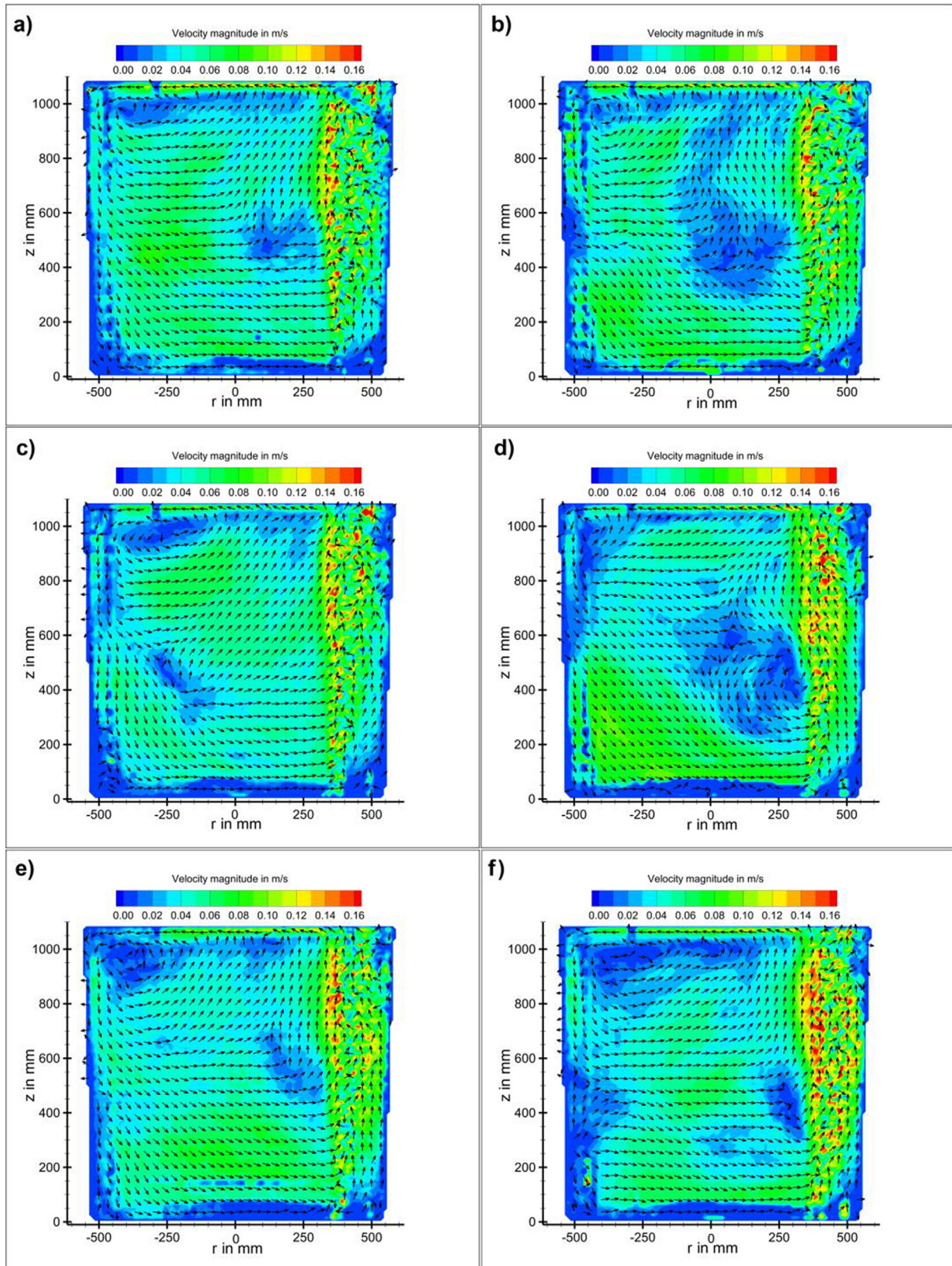


Fig. 6. Cross-section A-A of the water model used for the PIV measurements. (a) Side view. (b) Top view.



**Fig. 7.** PIV results for velocity magnitude (m/s, at cross-section A-A) with a cut-off filter and  $Q = 16.7$  slm. (a) Case I, (b) Case II, (c) Case III, (d) Case IV (e) Case V and (f) Case VI.

plume. At the upper left corner, a circulation can be observed in all measurements, transferring some of the liquid's momentum into the deeper regions of the ladle and other towards the plume region or the free surface. The momentum transfer into the deeper

regions, combined with the sucking of liquid into the plume causes the characteristic circulating flow. This is in accordance with Joo and Guthrie [24], who reported the presence of a circulating flow in an earlier study. In Case I, the velocity magnitude is highest,

whereas it is lowest in Case VI. Areas with almost no convection are present, known as 'dead zones', can be found for all injectors, though their location and size differ. The two flow fields obtained with the porous plug, either with a reduced diameter or with the

full diameter, are quite similar, but the area with a lower velocity magnitude is more pronounced in Case II. Using plate injectors, the flow field alters significantly but shows generally lower velocity magnitudes.

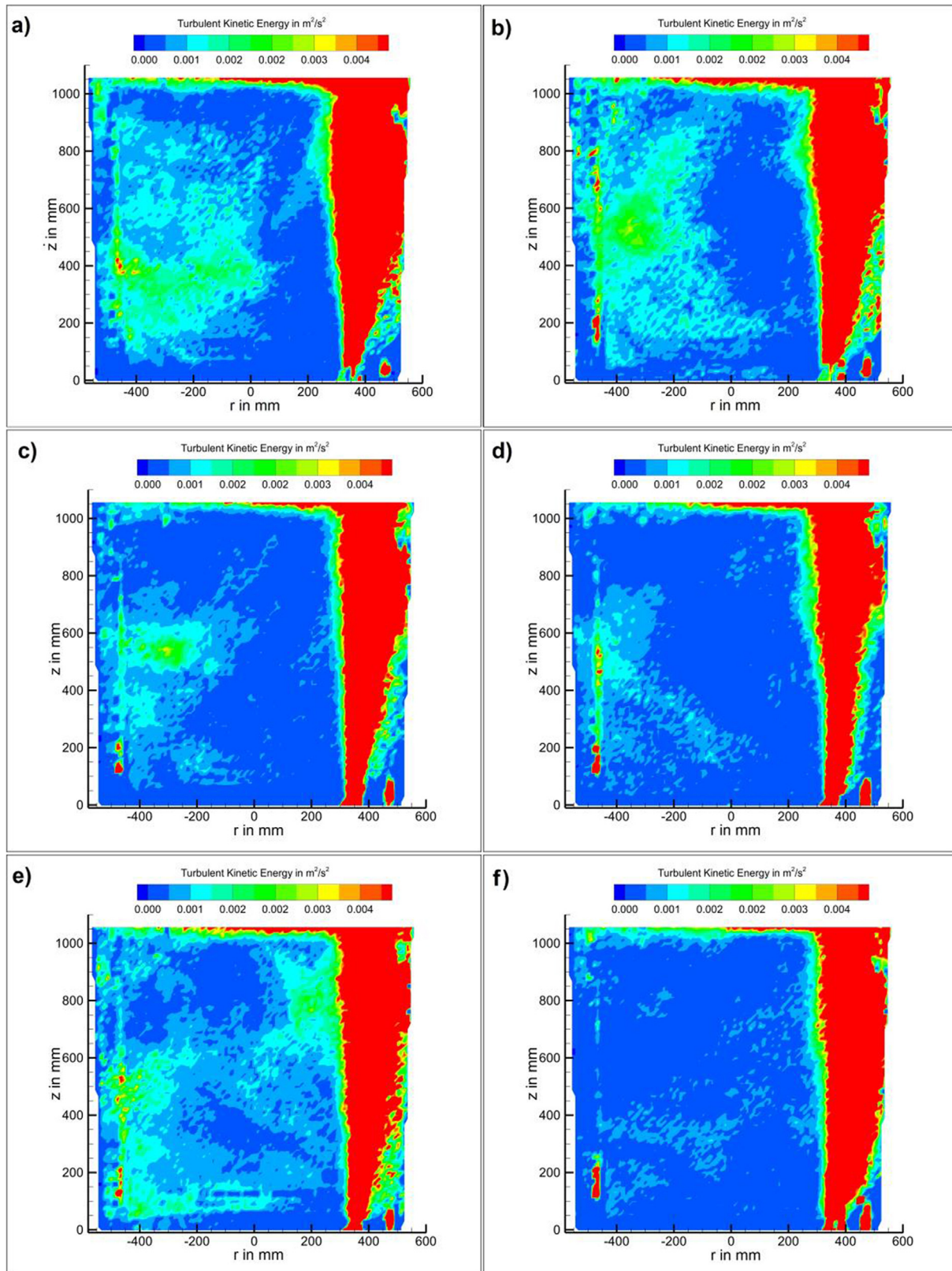


**Fig. 8.** PIV results for turbulent kinetic energy ( $\text{m}^2/\text{s}^2$ ), at cross-section A-A with a cut-off filter and  $Q = 16.7$  slm. (a) Case I, (b) Case II, (c) Case III, (d) Case IV, (e) Case V and (f) Case VI.

### 3.3. PIV: turbulent kinetic energy (TKE)

More than bulk convection, the turbulent diffusion was identified as a relevant factor for the mixing time. However, since the turbulent diffusion is difficult to measure, the turbulent kinetic energy was taken as an indirect measure of the degree of turbulence that can be derived from the PIV measurements. The TKE is estimated from the average instantaneous flow field velocity as follows [42]:

$$E_{tke} = \frac{1}{2} |V_{rms}|^2 [\text{m}^2 \text{ s}^{-2}] \quad (6)$$

$V_x$  and  $V_z$  each add a  $1/4 V_{rms}^2$ ,

$$E_{tke} = 1/2 V_{rms}^2 + 1/4 V_{rms}^2 = 3/4 V_{rms}^2 \quad (7)$$

where  $E_{tke}$  is the TKE and  $V_{rms}$  are velocity vector fields.

The results provide a single value that represents all the velocity components at each point. TKE data results are exported, analyzed and visualized using TecPlot EX 2017 R software. The results for the different injectors at the same flow rate of 16.7 slm are presented in Fig. 8. Again, the plume and the adhesive seam area cannot be evaluated. The structure of turbulent kinetic energy can roughly be correlated with the magnitude of the flow field, since the fluid's ability to dampen turbulent disturbances declines with higher flow velocities. Similarly, as for the velocity magnitude, the porous plugs produce the highest turbulent kinetic energy. The lowest magnitude was found for the plate with five orifices in a row.

## 4. Discussion

Since convective flow and turbulent diffusion are essential in the gas stirred ladle [20,43], both phenomena are investigated and compared with the measured mixing times. It is shown that the different injector types yield very similar mixing times with a relative deviation of 6.4%. Thus, it can be concluded that it plays a minor role in process optimization. The application of a porous plug seems to slightly lower the mixing time, while the reduction of the plug's diameter has almost no effect. This result is in contrast to that of Krishna Murthy et al. [15], who found that the mixing time is decreased in Case II. This can be explained by the flow field, of which the structure and magnitude change very little between the two cases. The bulk convection and the turbulent kinetic energy were slightly lower in the cases where PVC plates were used (Cases III, IV, V, and VI). Owing to that, the mixing time was increased. Whether bulk convection or turbulent diffusion is the predominant phenomenon cannot be conclusively stated since the transport mechanisms are co-dependent. Since the applied PIV technique only allowed 2D measurements, no comprehensive conclusion for the overall flow in the whole ladle can be made. Thus, it is possible, that the differences between Cases V and VI can be explained by flow structures oriented perpendicular to the depicted symmetry plane. The additional measurement, in which the position of the tracer injection was altered, showed that the injection position is a crucial factor for the mixing time measurements. This could be due to the changed path along which the tracer needs to be transported, or due to the tracer being injected into a zone of weak convection within the inhomogeneous structure of the flow. The position of the 'dead zones' depends upon the type of injector used. The large variation of the mixing time obtained with the same type of injector proved that the position of tracer injection has a significant influence on the measured mixing time, as it was found in earlier studies [9,22,25]. As reported in the literature [22], the plume is slightly deflected towards the sidewall. Thus, the erosion of the sidewall can be enhanced. This effect was most pronounced in Cases I and VI.

## 5. Conclusion

A water model of ratio 1/3 was modeled from an industrial 185 t gas stirred ladle. An eccentric porous plug was mounted with various types of perforated plates made of PVC. Experiments have been conducted to investigate the influence of individual plates on the mixing time via continuous tracer addition at a constant gas flow rate of 16.7 slm. The results of the mixing time measurements were correlated with the bulk convection and turbulent kinetic energy derived from Particle Image Velocimetry (PIV) results. The position of the tracer injection was altered to observe the impact on the mixing time. The results can be summarized as follows:

- Even though some differences can be found in terms of bulk convection and turbulent kinetic energy, the relative deviation in mixing time for all tested injectors is 6.4%. The porous plug (Cases I and II) yields the shortest mixing time, independent of its diameter.
- The experiments in which the tracer injection position was altered, show a significant variation in the mixing time. It can be concluded that the position of the injection, as well as the probing positions, are crucial factors in the investigation of the mixing behavior. Owing to that, it is highly important to retain exactly the same positions throughout all experiments.
- The analysis of the PIV measurements reveals that the bulk convection and the turbulent kinetic energy can be correlated with the mixing time. Consequently, these transport mechanisms are determining factors. To which extend the different phenomena account for the mixing cannot be conclusively stated though, since they are not independent of one another.
- Compared to other determining factors like the plug eccentricity, bath height or gas flow rate, the type of injector seems to have a minor effect on the mixing behavior of the ladle.

## Acknowledgments

Proofreading by Ms. Suzanne Roberts is gratefully acknowledged. This work was funded by the German Research Foundation (Deutsche Forschungsgemeinschaft (DFG)) within the project RU 2050/2-1. The authors would like to express sincere thanks to the officials of the TGGs, KMUTNB, IOB and RWTH Aachen institutions for the support, also to the German Academic Exchange Service (Deutscher Akademischer Austauschdienst (DAAD)) for partial financial support of the abroad research studies of P. Gajjar and K.B. Owusu.

## Declarations of interest

The authors declare no conflict of interest.

## Appendix

**Capacity utilization ratio:** The monthly crude steel capacity utilization ratio is calculated based on crude steel production information available at worldsteel and Organization for Economic Co-operation and Development (OECD) capacity estimates.

$$\text{Capacity utilization ratio} = \left( \frac{\text{Current production of given month}}{\frac{\text{Yearly production}}{\text{No of days in year}} \cdot \text{No of days in given month}} \right) \cdot 100$$

1. Take the OECD estimate of global steelmaking capacity and divide it by the number of days in the particular year ( $\frac{2,380.7}{365} = 6.5$ ).
2. Multiply it with the number of days of the month in question ( $6.5 \cdot 30$  (in June) = 195).

## Descriptive diagram of all cases used in Experiment:

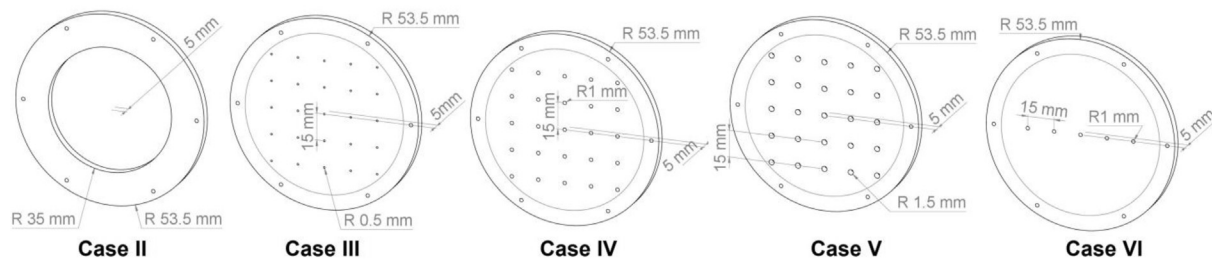


Fig. 9.

3. Divide the given month's production figure by the figure above and multiply by 100 ( $\frac{154.8}{195} \cdot 100 = 79.1$ ).
4. This figure differs from the given figure of 77.7% because on a monthly basis it only receives the production estimates of 64 countries, not all the steel producing countries in the world. The figure is adjusted slightly to reflect production estimates from the remaining countries.
5. 64 countries (accounted for approximately 99% of total world crude steel production): Argentina, Australia, Austria, Belarus, Belgium, Bosnia-Herzegovina, Brazil, Bulgaria, Canada, Chile, China, Colombia, Croatia, Cuba, Czech Republic, Ecuador, Egypt, El Salvador, Finland, France, Germany, Greece, Guatemala, Hungary, India, Iran, Italy, Japan, Kazakhstan, Libya, Luxembourg, Macedonia, Mexico, Moldova, Netherlands, New Zealand, Norway, Pakistan, Paraguay, Peru, Poland, Portugal, Qatar, Romania, Russia, Saudi Arabia, Serbia, Slovakia, Slovenia, South Africa, South Korea, Spain, Sweden, Taiwan, Thailand, Turkey, Ukraine, United Arab Emirates, United Kingdom, United States, Uruguay, Uzbekistan, Venezuela and Vietnam.

## Descriptive diagram of all cases used in Experiment:

See Fig. 9.

## References

- [1] World Steel in Figures 2018, World Steel Association AISBL Belgium, <https://www.worldsteel.org/media-centre/press-releases/2018/world-steel-in-figures-2018.html>, 2018 (accessed 7 August 2018).
- [2] May 2018 Crude Steel Production, World Steel Association AISBL Belgium, <https://www.worldsteel.org/media-centre/press-releases/2018/may-2018-crude-steel-production.html>, 2018 (accessed 7 August 2018).
- [3] D. Mazumdar, R.I. Guthrie, The physical and mathematical modelling of gas stirred ladle systems, *ISIJ Int.* 35 (1995) 1–20.
- [4] T. Haiyan, G. Xiaochen, W. Guanghui, W. Yong, Effect of gas blown modes on mixing phenomena in a bottom stirring ladle with dual plugs, *ISIJ Int.* 56 (2016) 2161–2170.
- [5] D. Mazumdar, P. Dhandapani, R. Sarvanakumar, Modeling and optimisation of gas stirred ladle systems, *ISIJ Int.* 57 (2017) 286–295.
- [6] J. Szekely, G. Carlsson, L. Helle, *Ladle Metallurgy*, Springer-Verlag, New York, 1989.
- [7] K. Nakanishi, T. Fujii, J. Szekely, Possible relationship between energy dissipation and agitation in steel-processing operations, *Ironmaking Steelmaking* 2 (3) (1975) 193–197.
- [8] R. Singh, Master Thesis, Indian Institute of Technology, Kanpur, 2007.
- [9] M.-Y. Zhu, T. Inomoto, I. Sawada, T.-C. Hsiao, Fluid flow and mixing phenomena in the ladle stirred by argon through multi-tuyere, *ISIJ Int.* 35 (1995) 472–479.
- [10] M. Iguchi, K.-I. Nakamura, R. Tsujino, Mixing time and fluid flow phenomena in liquids of varying kinematic viscosities agitated by bottom gas injection, *Metall. Mater. Trans. B* 29 (1998) 569–575.
- [11] A.M. Amaro-Villeda, M.A. Ramirez-Argaez, A.N. Conejo, Effect of slag properties on mixing phenomena in gas-stirred ladles by physical modeling, *ISIJ Int.* 54 (2014) 1–8.
- [12] D. Mazumdar, R.I. Guthrie, Mixing models for gas stirred metallurgical reactors, *Metall. Trans. B* 17 (1986) 725–733.
- [13] J. Mietz, F. Oeters, Flow field and mixing with eccentric gas stirring, *Steel Res. Int.* 60 (1989) 387–394.
- [14] T. Stapurewicz, N.J. Themelis, Mixing and mass transfer phenomena in bottom-injected gas-liquid reactors, *Can. Metall. Q.* 26 (1987) 123–128.
- [15] G. Krishna Murthy, S. Mehrotra, A. Ghosh, Experimental investigation of mixing phenomena in a gas stirred liquid bath, *Metall. Trans. B* 19 (1988) 839–850.
- [16] S. Asai, T. Okamoto, J.C. He, I. Muchi, Mixing time of refining vessels stirred by gas injection, *Trans. Iron Steel Inst. Jpn.* 23 (1983) 43–50.
- [17] R. González-Bernal, G. Solorio-Díaz, A. Ramos-Banderas, E. Torres-Alonso, C.A. Hernández-Bocanegra, R. Zenit, Effect of the fluid-dynamic structure on the mixing time of a ladle furnace, *Steel Res. Int.* 89 (2018) 1700281.
- [18] U. Sinha, M. McNallan, Mixing in ladles by vertical injection of gas and gas-particle jets – a water model study, *Metall. Mater. Trans. B* 16 (1985) 850–853.
- [19] L. Helle, The calculation of the time required to mix liquid metal in a ladle by gas rinsing, *J. Southern Afr. Inst. Mining Metall.* 81 (1981) 329–337.
- [20] D. Mazumdar, R.I. Guthrie, Considerations concerning the numerical computation of mixing times in steelmaking ladles, *ISIJ Int.* 33 (1993) 513–516.
- [21] G.K. Murthy, Mathematical modelling and simulation of recirculatory flow as well as mixing phenomena in gas stirred liquid baths, *ISIJ Int.* 29 (1989) 49–57.
- [22] W. Lou, M. Zhu, Numerical Simulation of desulfurization behavior in gas-stirred systems based on computation fluid dynamics-simultaneous reaction model (CFD–SRM) coupled model, *Metall. Mater. Trans. B* 45 (2014) 1706–1722.
- [23] J. Mandal, S. Patil, M. Madan, D. Mazumdar, Mixing time and correlation for ladles stirred with dual porous plugs, *Metall. Mater. Trans. B* 36 (2005) 479–487.
- [24] S. Joo, R. Guthrie, Modeling flows and mixing in steelmaking ladles designed for single-and dual-plug bubbling operations, *Metall. Trans. B* 23 (1992) 765–778.
- [25] C. Chen, Q. Rui, G. Cheng, Effect of salt tracer amount on the mixing time measurement in a hydrodynamic model of gas-stirred ladle system, *Steel Res. Int.* 84 (2013) 900–907.
- [26] T.-Y. Kuo, J.-C. Kuo, Determination of mixing time in a ladle-refining process using optical image processing, *ISIJ Int.* 51 (2011) 1597–1600.
- [27] D.-Q. Geng, H. Lei, J.-C. He, Optimization of mixing time in a ladle with dual plugs, *Int. J. Miner. Metall. Mater.* 17 (2010) 709–714.
- [28] Z. Liu, L. Li, B. Li, Modeling of gas-steel-slag three-phase flow in ladle metallurgy: Part I. Physical modeling, *ISIJ Int.* 57 (2017) 1971–1979.
- [29] S.-H. Kim, R. Fruehan, Physical modeling of liquid/liquid mass transfer in gas stirred ladles, *Metall. Mater. Trans. B* 18 (1987) 381–390.
- [30] D. Mazumdar, H. Nakajima, R. Guthrie, Possible roles of upper slag phases on the fluid dynamics of gas stirred ladles, *Metall. Trans. B* 19 (1988) 507–511.
- [31] O. Haida, J.K. Brimacombe, Physical-model study of solute inhomogeneity in injection refining processes, refining of iron and steel by powder injection, *SCANINJECT III* 1 (1983) 5.
- [32] L. Lehr, Gas agitation of liquids, *Ind. Eng. Chem. Process Des. Dev.* 7 (1968) 226–239.
- [33] M. Sano, K. Mori, Fluid flow and mixing characteristics in a gas-stirred molten metal bath, *Trans. Iron Steel Inst. Jpn.* 23 (1983) 169–175.
- [34] J. Mietz, F. Oeters, Model experiments on mixing phenomena in gas-stirred melts, *Steel Res. Int.* 59 (2) (1988) 52–59.
- [35] J. Mietz, F. Oeters, Flow field and mixing with eccentric gas stirring, *Steel Res. Int.* 60 (9) (1989) 387–394.
- [36] C.G. Méndez, N. Nigro, A. Cardona, S.S. Begnis, W.P. Chiapparoli, *Mecán. comput.* 21 (2002) 2646.
- [37] T. Haas, A. Rueckert, A.H. Pfeifer, Numerical modelling of the bubble driven flow within a steel ladle validated by particle image velocimetry, in: 7th International Conference on Modelling and Simulation of Metallurgical Processes in Steelmaking (STEELSIM2017), Qingdao, China (August 2017), p. 7.
- [38] L. Li, Z. Liu, B. Li, H. Matsuura, F. Tsukihashi, Water model and CFD-PBM coupled model of gas-liquid-slag three-phase flow in ladle metallurgy, *ISIJ Int.* 55 (2015) 1337–1346.
- [39] P. Ternstedt, A. Tilliander, P.G. Jönsson, M. Iguchi, Mixing time in a side-blown converter, *ISIJ Int.* 50 (2010) 663–667.
- [40] N. Kochi, K. Mori, Y. Sasaki, M. Iguchi, Mixing time in a bath in the presence of swirl motion induced by horizontal gas injection with an L-shaped lance, *ISIJ Int.* 51 (2011) 344–349.
- [41] C. Wuppermann, N. Giesselmann, A. Rückert, H. Pfeifer, H.-J. Odenthal, E. Hovestädt, A novel approach to determine the mixing time in a water model of an AOD converter, *ISIJ Int.* 52 (2012) 1817–1823.
- [42] DaVis 8.1 Manual, [https://istina.msu.ru/media/equipment/files/2015/10/06/1003001\\_DaVis\\_D81.pdf](https://istina.msu.ru/media/equipment/files/2015/10/06/1003001_DaVis_D81.pdf), (accessed 7 August 2018).
- [43] D. Mazumdar, Doctoral Thesis, Department of Mining and Metallurgical Engineering, McGill University, Montreal, 1985.